ISPRS Journal of Photogrammetry and Remote Sensing 128 (2017) 158–169

Contents lists available at ScienceDirect

ISPRS Journal of Photogrammetry and Remote Sensing

journal homepage: www.elsevier.com/locate/isprsjprs

Using spectrotemporal indices to improve the fruit-tree crop classification accuracy

M.A. Peña [a,b,*], R. Liao [c], A. Brenning [b,c]

[a] Departamento de Geografía, Universidad Alberto Hurtado, Cienfuegos 41, Santiago, Chile
[b] Department of Geography, Friedrich Schiller University Jena, Löbdergraben 32, 07737 Jena, Germany
[c] Department of Geography and Environmental Management, University of Waterloo, 200 University Ave W, Waterloo, Ontario N2L 3G1, Canada

ARTICLE INFO

Article history:
Received 2 November 2016
Received in revised form 27 March 2017
Accepted 29 March 2017

Keywords:
Satellite image time series
Spectrotemporal indices
Landsat-8
Linear discriminant analysis
Crop type classification

ABSTRACT

This study assesses the potential of spectrotemporal indices derived from satellite image time series (SITS) to improve the classification accuracy of fruit-tree crops. Six major fruit-tree crop types in the Aconcagua Valley, Chile, were classified by applying various linear discriminant analysis (LDA) techniques on a Landsat-8 time series of nine images corresponding to the 2014–15 growing season. As features we not only used the complete spectral resolution of the SITS, but also all possible normalized difference indices (NDIs) that can be constructed from any two bands of the time series, a novel approach to derive features from SITS. Due to the high dimensionality of this "enhanced" feature set we used the lasso and ridge penalized variants of LDA (PLDA). Although classification accuracies yielded by the standard LDA applied on the full-band SITS were good (misclassification error rate, MER = 0.13), they were further improved by 23% (MER = 0.10) with ridge PLDA using the enhanced feature set. The most important bands to discriminate the crops of interest were mainly concentrated on the first two image dates of the time series, corresponding to the crops' greenup stage. Despite the high predictor weights provided by the red and near infrared bands, typically used to construct greenness spectral indices, other spectral regions were also found important for the discrimination, such as the shortwave infrared band at 2.11–2.19 μm, sensitive to foliar water changes. These findings support the usefulness of spectrotemporal indices in the context of SITS-based crop type classifications, which until now have been mainly constructed by the arithmetic combination of two bands of the same image date in order to derive greenness temporal profiles like those from the normalized difference vegetation index.

1. Introduction

Remote sensing-based crop classification refers to the procedure through which different crop types are discriminated from imagery based on their spectral behavior throughout the optical spectrum. If the classification result is accurate enough, this procedure may contribute to efficiently designing and updating crop inventories. Nonetheless, to achieve that goal may be challenging as many crop types may exhibit similar spectral behavior during some phenological stages, particularly at the spectral resolution and bandwidth of multispectral images often used to perform the classification (Esch et al., 2014; McCoy, 2005). The accuracy of such procedures may therefore be strongly limited if just a single image acquired within a spectrally unsuitable temporal window is used (Jewell, 1989; Lo et al., 1986; Murakami et al., 2001; Van Niel and McVicar, 2004).

To deal with this shortcoming, a temporal sequence of images acquired at different dates across the entire growing season of the crops of interest (usually from spaceborne optical sensors) may be used, i.e., a satellite image time series (SITS). By using SITS the chances of successfully classifying crop types may increase as at different phenological stages they may exhibit distinct timings, which will likely translate into spectrotemporal separabilities that will favor their discrimination (Lo et al., 1986; Chen et al., 2008). SITS have been used widely to classify crop types, taking advantage of the spatially and temporally frequent image acquisitions made by the increasing number of Earth-observing satellites. The most common approach has been the retrieval of NDVI (normalized difference vegetation index) temporal profiles from a time series

* Corresponding author at: Departamento de Geografía, Universidad Alberto Hurtado, Cienfuegos 41, Santiago, Chile.
E-mail addresses: mapena@uahurtado.cl, marco.pena@uni-jena.de (M.A. Peña), r2liao@uwaterloo.ca (R. Liao), alexander.brenning@uni-jena.de, alexander.brenning@uwaterloo.ca (A. Brenning).

http://dx.doi.org/10.1016/j.isprsjprs.2017.03.019

corresponding to the crops' growing season, thus providing a synthetic measure of the vegetation vigor or greenness across its main phenological stages (Odenweller and Johnson, 1984; Jones and Vaughan, 2010).

Most of the NDVI temporal profiles used for crop type classification purposes have been constructed from MODIS-derived NDVI composites, prepared and distributed by the Center for Earth Resources Observation and Science (EROS) of the USGS (United States Geological Survey) (Jakubauskas et al., 2002; Sakamoto et al., 2005; Xavier et al., 2006; Shao et al., 2010; Mingwei et al., 2008; Masialeti et al., 2010; Wardlow and Egbert, 2010; Arvor et al., 2011; Chenab et al., 2011; Zhong et al., 2011; Sibanda and Murwira, 2012; Sun et al., 2012). There are several reasons explaining the wide use of these products, among these: they record 16- or 32-days NDVI maximum, which increases the chances of depicting cloud-free areas. They are radiometrically processed, so no further corrections are needed. They cover large areas, reducing the need to mosaicking images with different illumination levels. Lastly, they are available for free from the website of the MODIS Science Team. In spite of these advantages, the use of MODIS-derived NDVI temporal profiles may be restrictive where crop fields are smaller than the MODIS image pixel size; ranging from 250 to 1000 m, depending on the NDVI composite. To overcome this limitation, an alternative may be to derive these profiles from a set of optical images with higher spatial resolution, like the ones acquired by the Landsat satellites (Badhwar et al., 1987; Turker and Arikan, 2005; Simonneaux et al., 2007; Zhong et al., 2014; Zheng et al., 2015). However, the Landsat's revisit period of 16 days increases the chances of missing some image dates due to excessive cloudiness, especially in humid climates. This issue may produce gaps across the NDVI temporal profile that could hinder the pursued classification.

Regardless of the optical images used, crop type classifications based on NDVI temporal profiles have yielded good results employing different classification algorithms (Arvor et al., 2011; Masialeti et al., 2010; Murakami et al., 2001; Ozdogan, 2010; Van Niel and McVicar, 2004; Zheng et al., 2015). Nonetheless, most of these studies have targeted graminaceous crops. These crops commonly have annual growth cycles with planting dates that may differ according to the species. As a consequence, they may exhibit distinctive budburst and greenup timings that facilitate their discrimination. Many of these crops are furthermore cultivated in annual rotations or double cropping systems. Therefore, they may exhibit distinctive harvesting and regrowth timings, which also aid in their discrimination. Instead, the classification of perennial crops like fruit-trees using NDVI temporal profiles has been addressed less frequently (Simonneaux et al., 2007; Zhong et al., 2011; Peña and Brenning, 2015). Unlike graminaceous crops, different fruit-tree crops may exhibit more similar mean timings in their phenological stages, making their discrimination a more challenging task, particularly if the image acquisition dates do not match with the stages at which inter-class spectral separability is maximized (Zhong et al., 2011).

It is noteworthy the lack of studies addressing crop type classifications by using the complete spectral resolution of SITS. Albeit it is not a new approach (see early references in Lo et al., 1986), few studies have been carried out during the last years (e.g., Van Niel and McVicar, 2004). It is reasonable to suppose that better classification accuracies can be achieved if all image bands (or spectral samples) throughout the time series are used as feature set instead of a greenness-related spectral index constructed from only two bands per image. This is simply because the full optical spectrum comprises wavelengths sensitive to vegetation properties other than greenness. For instance, short-wave infrared (SWIR) bands have been widely used as indicators of foliar water content and there are findings supporting their uncorrelatedness with greenness-related bands (Ceccato et al., 2001, 2002). Moreover, many optical sensors allow to construct a water content spectral index named NDWI (normalized difference water index), which is formulated in a similar way as the NDVI, but replacing the red band with a SWIR band centered around 1.24 μm (Gao, 1996). However, the application of this spectral index for SITS-based crop type classification purposes has been largely disregarded (Peña and Brenning, 2015).

Although using the full-band SITS may increase the chances of discriminating crop types, it also poses the challenge of efficiently processing large and eventually high-dimensional feature sets. In recent years, machine learning techniques have shown good capabilities to extract meaningful information from hyperspectral remote sensing data, which require dealing with hundreds of correlated bands, usually using limited training sets (Mountrakis et al., 2011; Bioucas-Dias et al., 2013). SITS are prone to producing spectral redundancies with increasing image and thus feature numbers. In SITS-based crop type classifications, correlations between bands may vary in time, depending on the image acquisition frequency and the phenology of the depicted crops. As with hyperspectral imaging, machine learning techniques may be applied to extract information from SITS-derived feature sets (Peña and Brenning, 2015). However, these techniques have been mostly used to detect changes on a limited number of land use/-cover types from a few image dates (Rodriguez-Galiano et al., 2012; Gómez et al., 2016) rather than to discriminate intraspecific classes, such as crop types, using larger SITS-derived feature sets.

Peña and Brenning (2015) classified four major fruit-tree crop types in central Chile applying different machine learning techniques and training sample sizes on a Landsat-8 time series. They used as feature sets both NDVI and NDWI temporal profiles, as well as the complete spectral resolution of the SITS. Classification accuracies, measured by cross-validation of the misclassification error rate (MER), were the best when using the full-band SITS (MER = 0.13–0.05), while NDVI temporal profiles had the worst overall performance (MER 4–13% higher than for full-band SITS and up to 3% worse than NDWI temporal profiles).

The present study assesses the classification of six major fruit-tree crop types in the Aconcagua Valley, central Chile, using a Landsat-8 time series corresponding to the 2014–15 growing season. The valley is inserted in the same climate region as the one studied by Peña and Brenning (2015), but exhibits different agrometeorological settings as well as fruit-tree species. We used as feature sets the full-band SITS and all the normalized difference indices (NDIs) possible of being constructed from any two bands of the SITS. The assumption regarding this NDI-based feature set was that it might contribute to improving the crop type classification as it comprises an extensive number of arithmetic band combinations from which distinct spectral signals may arise for different crop types.

Feature sets comprising all possible NDIs have been constructed from hyperspectral data to empirically relate them to canopy structure variables of native forest species (Peña et al., 2012) or to different crop diseases (Mahlein et al., 2013). Nonetheless, to our knowledge this is the first time that this type of feature set is used in the context of SITS-based classifications. Considering the findings of Peña and Brenning (2015), we decided to perform the classifications of interest using only linear discriminant analysis (LDA), as it had a superior performance than some other state-of-the-art machine learning techniques. In that study LDA was applied to classify similar crops as the targeted by us (fruit-trees) and from a time series comprised of Landsat-8 images as well. Nonetheless, to deal with the collinearity of the high-dimensional NDI-based feature set, in the present study we additionally consider two penalized LDA (PLDA) variants, which have shown their suitability to deal with hyperspectral imagery

by shrinking and reducing their intrinsic high dimensionality (Du and Younan, 2008).

2. Materials and methods

2.1. Study area

The study area corresponds to agricultural land located in the Andean foothills of the Aconcagua River basin, Valparaiso Region, Chile, one of largest watersheds in the country (7340 km^2). The climate is Mediterranean, with hot, dry summers and cool, wet winters. Its hydrological regime is controlled by snowmelt in the Andean headwaters in spring and rainfall in winter. Agriculture is the prevailing land use on the valley floor and its fluvial terraces (862 km^2) (INE, Instituto Nacional de Estadísticas, 2008). The study area includes four counties (Petorca, Calle Larga, Los Andes and Zapallar) with a total area of 576 km^2. We targeted its most common crops: table grape (*Vitis vinifera* L.), walnut (*Juglans regia* L.), peach (*Prunus persica* L.), avocado (*Persea americana* Mill.), nectarine (*Prunus persica* var. nectarine) and mandarin (*Citrus reticulata* Blanco) (Fig. 1 and Table 1). These fruit-tree crops are cultivated on relatively small fields (N = 5233; mean size 38,390 m^2) heterogeneously arranged between the cities of Los Andes and San Felipe and around the Aconcagua River. Their growing season broadly ranges from late September (greenup stage in southern spring) to early April (senescence stage in southern autumn), showing shifts of several days in their onset and offset timings depending on the specific crop variety and management practices.

Table 1
Area occupied by the six targeted fruit-tree crops and other fruit trees cultivated in the study area.

Fruit-tree crop	Area	
	km^2	%
Table grape	96.4	53.6
Walnut	42.2	23.5
Peach	25.9	14.4
Avocado	7.2	4.0
Nectarine	2.9	1.6
Mandarin	2.1	1.1
Others	3.1	1.7
Total	179.8	100

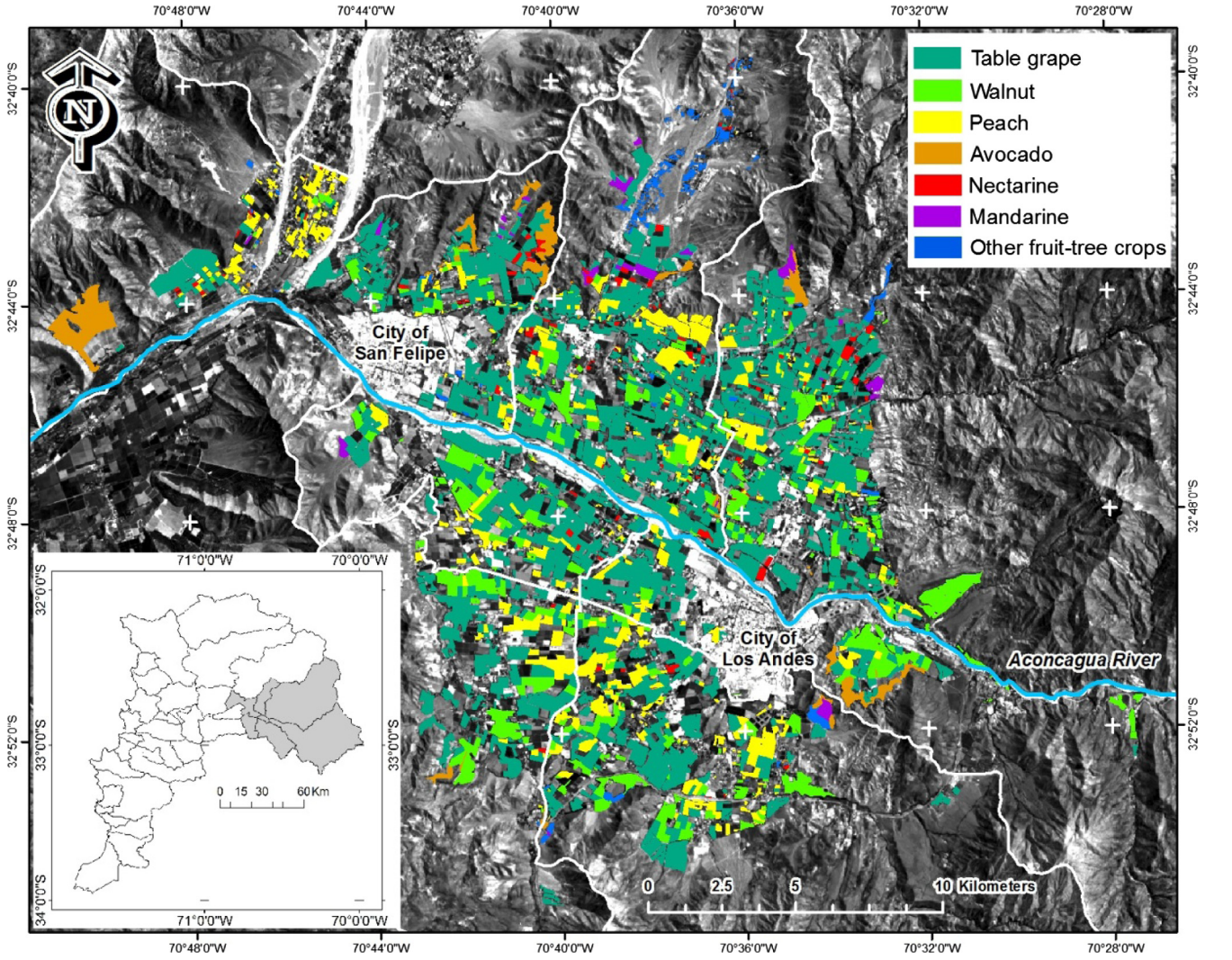

Fig. 1. Distribution of the target fruit-tree crops within the study area, corresponding to a section of the Aconcagua Valley, central Chile. White lines denote county boundaries. The embedded image shows the county boundaries of the Region of Valparaíso, highlighting in gray those in which the study area is inserted.

2.2. Satellite image time series construction

A SITS was constructed with all cloud-free Landsat-8 images acquired during the 2014–15 growing season. All images covering the study area were acquired on the same orbital path and row number (233/83) with a temporal frequency of 16 days (the revisit period of the satellite). The images were selected and downloaded from the Global Visualization Viewer (http://glovis.usgs.gov) of the USGS (Table 2). Landsat-8 was launched on February 11th, 2013, carrying the pushbroom sensor OLI (Operational Land Imager), which samples the optical spectrum in nine bands. In this study, the panchromatic band 8 (0.5–0.68 μm) was not used because of its broad spectral width. Neither band 1 (0.43–0.45 μm) nor 9 (1.36–1.39 μm) was used because they were designed for coastal water and atmospheric aerosol applications (Roy et al., 2014). Meanwhile, thermal bands 10 (10.60–11.19 μm) and 11 (11.50–12.51 μm) acquired by the TIRS (Thermal Infrared Sensor) instrument on board this satellite were also discarded, mainly because of their relatively large original image pixel size of 100 m, which fails to clearly depict most of the crop fields of interest. Table 3 lists the main technical characteristics of the Landsat-8 OLI bands used in this study.

2.3. Satellite image time series pre-processing

Landsat-8 images are originally distributed by the USGS after geometric correction, a product named Level 1 terrain corrected (L1T). The procedures include a systematic geometric correction as well as the use of ground control chips and a digital elevation model (DEM) to further improve the image geometry, resulting in a circular geolocation error below 12 m with 90% confidence (Roy et al., 2014). The default image output coordinate system is Universal Transverse Mercator (UTM) with World Geodetic System 1984 (WGS84) datum. We additionally verified the proper spatial coregistration of the SITS by examining the spatial match between some randomly selected crops fields across different images, and we found only negligible spatial shifts in their boundaries (below half pixel).

The digital numbers of the images were converted into *exo*-atmospheric radiances by applying the radiometric calibration parameters of the OLI bands, available in ENVI© (Environment for Visualizing Images) 5.0.3 software (Exelis Visual Information Solutions, Inc., Boulder, USA). Thereafter, these radiances were converted to surface apparent reflectances using the FLAASH (Fast Line-of-Sight Atmospheric Analysis of Spectral Hypercubes) module available in the mentioned software. This is a MODTRAN® (Moderate Resolution Atmospheric Transmission, Spectral Sciences, Inc., Burlington, USA) based algorithm that allows modeling the at-surface irradiance and at-surface radiance of the image's pixels by taking into account a set of user-defined scene and atmosphere parameters.

Table 2
Acquisition dates of the Landsat-8 images used in this study.

Image		Season in the study area
#	Acquisition date	
1	August 6, 2014	Autumn
2	September 6, 2014	Autumn
3	October 24, 2014	Spring
4	January 12, 2015	Summer
5	January 28, 2015	Summer
6	February 13, 2015	Summer
7	March 1, 2015	Summer
8	March 17, 2015	Summer
9	April 2, 2015	Autumn

2.4. Classification training and validation

The crop field database required to train the classifiers and to validate their results was constructed from the Fruit Cadastre of the study area, carried out by Chile's Agrarian Policies and Studies Bureau (Oficina de Estudios y Políticas Agrarias, ODEPA). This is an online cartography (http://odepa.cl) that shows the fruit-tree crop field boundaries of the Region of Valparaíso, updated to the 2013–14 growing season. The database was constructed by creating an inventory of fruit-tree crop fields of the region presenting at least 50 plants. It is updated every six years by field campaigns where the fruit-tree species planted on each of the fields mapped on the original database are verified while new fields are added to and inexistent fields are removed from the database (CIREN, 2014). To avoid the inclusion of mixed edge pixels during the selection of training areas, fields smaller than 22,500 m^2 (equivalent to the size of 5×5 Landsat pixels) or with a too narrow shape were removed from the original database. Furthermore, pixels with low vegetation cover were eliminated. As a consequence, the number of fields (polygons) and pixels used to classify the crop types was somewhat reduced (Table 4). Within the cross-validation procedure described below, stratified random samples of 200 fields were drawn as training sets from the available 3664 fields since this sample size produced nearly optimal accuracies in fruit-tree crop classification with LDA in a comparable earlier study (Peña and Brenning, 2015).

We used as classification features all the 54 bands of the SITS, referred to as the "baseline" feature set. Additionally, we created a second "enhanced" feature set by adding to the baseline feature set all the NDIs that can be constructed from any two bands of the SITS. An NDI arithmetically combines two bands in the form of the ratio of their difference and their sum: (band 1-band 2)/(band 1 + band 2). It ideally utilizes a band sensitive to a given response variable (band 1), and another one insensitive or inversely proportional to changes in such variable (band 2), which serves as control of potential confounding factors in the sensitive signal (Jones and Vaughan, 2010). Because of their formulation an NDI compensates illumination differences while constraining the values to a scale from -1 to 1. An example of an NDI is the previously mentioned NDVI, constructed with the NIR band (sensitive signal) and the red band (control signal) to predict variables related to vegetation vigor. For k bands, there are $k(k\text{-}1)/2$ possible NDIs considering that

Table 3
Main technical characteristics of the Landsat-8 OLI (Operational Land Imager) bands used in this study.

Band				
#	Spectral region	Spectral width (μm)	Spatial resolution (m)	Radiometric resolution (bits)
2	Blue	0.45–0.51	30 m	12
3	Green	0.53–0.59		
4	Red	0.64–0.67		
5	Near Infrared	0.85–0.88		
6	Shortwave infrared	1.57–1.65		
7	Shortwave infrared	2.11–2.19		

Table 4
Data used to classify the crops of interest. The original number of fields (second column) was somewhat reduced after removing too small or narrow fields (third column).

Crop type	Original number of fields (polygons)	Fields used				
		#		Area (m^2)		
		Polygons	Pixels	Mean	Standard deviation	Total
Table grape	3361	2808	4716	39,557	15,181	77,611,529
Walnut	613	359	1498	64,694	65,850	23,225,170
Peach	925	348	2408	45,489	30,241	15,830,244
Avocado	93	52	533	13,1147	155,495	6,819,634
Nectarine	193	50	274	34,450	14,241	1,722,521
Mandarin	48	37	248	51,335	35,571	1,899,402
Total	5233	3664	9677	45,267	38,820	127,108,500

changing the order of the bands used in NDI calculation merely changes the sign. Accordingly, the enhanced feature set consisted of 1431 features.

Classification performances were validated using spatial cross-validation (Brenning, 2012; Peña and Brenning, 2015). In cross-validation, the data set is divided into k equally-sized disjoint subsets (here: $k = 10$). All but one of the subsets is combined into a training set, and the trained classifier is then evaluated on the remaining subset. Each subset is used once as a test set, and the MER is calculated from the combined test-set predictions. This procedure is repeated 100 times in order to obtain results that are independent of the specific random partitioning. Since pixels from the same field share the same crop characteristics and soil background, they should be considered as pseudoreplications. Cross-validation was therefore performed by resampling fields, not pixels, in order to ensure that pixels from the same field are jointly placed in either the test or the training set. The implementation in the R package "sperrorest" was used (Brenning, 2012).

2.5. Linear discriminant analysis and penalized variants

Standard LDA and its lasso and ridge penalized variants were used in this study to assess the classification of the crops of interest while addressing the high dimensionality of the SITS-derived feature sets. As previously mentioned, we selected LDA because it compared favorably to computationally more demanding machine learning techniques in a similar study (Peña and Brenning, 2015) as well as in other benchmarking exercises that will be discussed later (Bandos et al., 2009; Brenning, 2009; Li et al., 2006; Yu et al., 1999).

LDA basically assumes that the joint distribution of the features conditional on the response class is a multivariate normal distribution with a common covariance matrix for all classes (see e.g. James et al., 2013). Using Bayes' theorem, this can be used to obtain linear decision boundaries based on LDA's linear discriminant functions. However, Fisher's standard LDA is not suitable for ill-posed high-dimensional problems with singular covariance matrices, which therefore require the use of regularized or penalized LDA techniques (Du and Younan, 2008). Lasso and ridge penalties are two contrasting approaches that use different norms in their penalty terms, the l_1 and l_2 norm, respectively. As a consequence, the lasso effectively penalizes some of the coefficients to (exactly) 0. It thus eliminates these variables from the model, which is not the case for ridge penalties. In both approaches a positive tuning parameter λ controls the degree of regularization, and lasso and ridge PLDA converge to the standard LDA as λ approaches 0. In this study, optimal λ values were determined using a nested cross-validation, i.e. within each of the outer cross-validation steps used for error estimation we performed an inner cross-validation on each training set to calculate error rates for varying λ ranging from 10^{-5} to 10^{2} for both lasso and ridge PLDA. Lasso PLDA and ridge PLDA implementations in the "penalizedLDA" and "mda" packages in R were used (Hastie et al., 1994, 1995; Witten and Tibshirani, 2011; R Core Team, 2014; Witten, 2015).

In order to assess the importance of different variables, the canonical coefficients in the first discriminant vector were retrieved and analyzed for the best-performing model. The first discriminant vector covered almost 50% of the between-group variance, while the second discriminant vector added only another 28%. Our variable importance assessment therefore was focused on the first discriminant vector. To be able to compare the canonical coefficients for different variables, they were multiplied with the corresponding variable's standard deviation (SD). These adjusted canonical coefficients are simply referred to as the coefficients.

The sensitivity of model coefficients and MERs to changes in λ were furthermore examined. To reduce random variability in this merely exploratory analysis, a larger stratified training sample of 817 fields was used for training, and all remaining fields for testing.

3. Results

3.1. Overall classification performance

Overall classification accuracies were good in general, with MER values ranging from 0.10 to 0.30 (Table 5). The best result was obtained by the ridge PLDA applied on the enhanced feature set (MER = 0.10) (Fig. 2). Ridge PLDA and LDA applied on the baseline feature set achieved nearly identical MERs (0.14 and 0.13, respectively). Lasso PLDA had the worst performance overall, yielding the highest MER (0.30) on the baseline feature set. The comparison of results within each classifier used revealed an improved performance of the enhanced feature set. This is particularly noticeable in the case of lasso PLDA, where the enhanced feature set yielded a MER 6 percentage points below the MER corresponding to the baseline feature set, which meant an error reduction of 20%. Similarly, the ridge PLDA applied on the enhanced feature set produced a MER 4 percentage points below the corresponding to the basic feature set, i.e. an error reduction of 28.6%.

As expected, the MER and SD of all the classifications were lower in the training set than in the validation set (Table 5). Ridge PLDA clearly overfitted the training set, especially when it was applied to the enhanced feature set, where it yielded an extraordinarily low MER compared to that of the test set (0.01 and 0.10, respectively). In spite of this, the ridge PLDA was also generalizable for the enhanced feature set and produced more accurate results.

3.2. Model selection

Focusing on ridge PLDA in the exploratory analysis of sensitivity to λ, the optimal MER was reached at $\lambda = 10^{-0.5} \approx 0.32$. The MER of 0.03 was lower than in the above analysis since a larger sample of 817 fields was used in this sensitivity analysis. This highlights the additional accuracy gains that can be achieved with large ground-truth sample sizes in this high-dimensional setting, as opposed to

Table 5
Overall cross-validated MERs (misclassification error rates) obtained from the standard and two PLDA (penalized linear discriminant analysis) classifiers applied on two feature sets derived from the Landsat-8 time series. MERs and their SDs (standard deviations) were calculated for training and test sets.

Classifier and feature set	Data set			
	Training		Test	
	MER	SD	MER	SD
Lasso PLDA and baseline feature set	0.27	0.01	0.3	0.03
Lasso PLDA and enhanced feature set	0.21	0.01	0.24	0.02
Ridge PLDA and baseline feature set	0.04	0.00	0.14	0.02
Ridge PLDA and enhanced feature set	0.01	0.00	0.10	0.02
LDA and baseline feature set	0.04	0.00	0.13	0.02

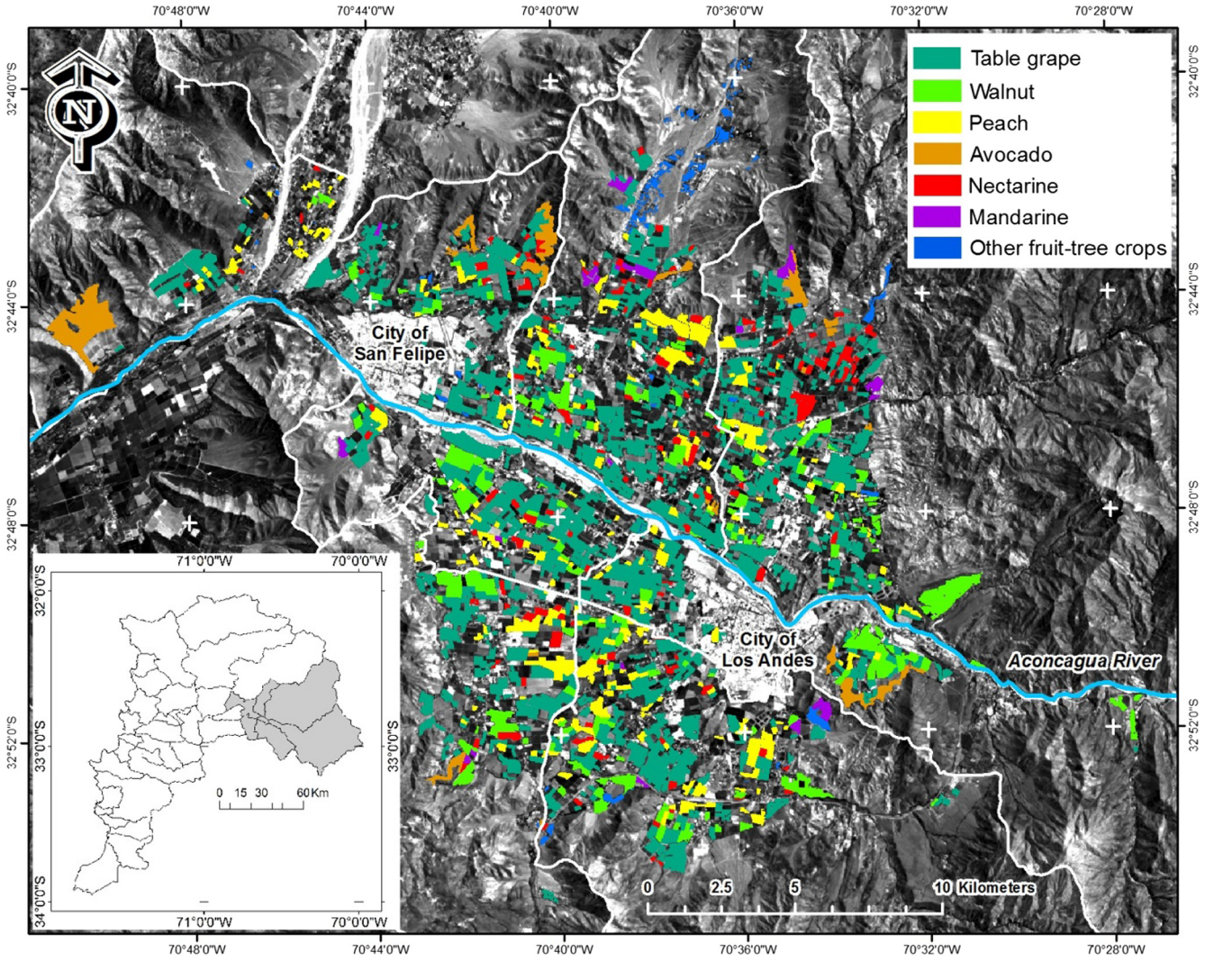

Fig. 2. Crop type classification using PLDA (penalized linear discriminant analysis) on the enhanced feature set. Fields previously removed because of their small size or narrow shape were not classified.

the lower-dimensional setting of Peña and Brenning (2015). The MER furthermore showed a secondary minimum at 10^{-4}. This is a very small penalty on the discriminant vectors, for which the ridge PLDA approaches a standard LDA. The MER also fluctuated, suggesting that the penalization algorithm was not stable (Bandos et al., 2009).

In ridge PLDA, five features representing the range of coefficient values were explored with respect to their change with increasing λ (Fig. 3). The coefficients changed their signs twice before gradually getting closer to zero, but their absolute values generally shrank towards 0 as λ increased.

In lasso PLDA, an optimal test-set MER of 0.16 was achieved at $\lambda = 10^{-4.25}$ and $10^{-3.5}$, although MER was nearly constant at this level for $\lambda \geq 10^{-1.5}$. A poor MER > 0.4 was obtained for larger values of λ.

The test-set confusion matrix of the classified crop types using the optimal ridge PLDA ($\lambda = 10^{-0.5}$) yielded good user's and producer's accuracies in all cases, except for nectarine (Table 6). For

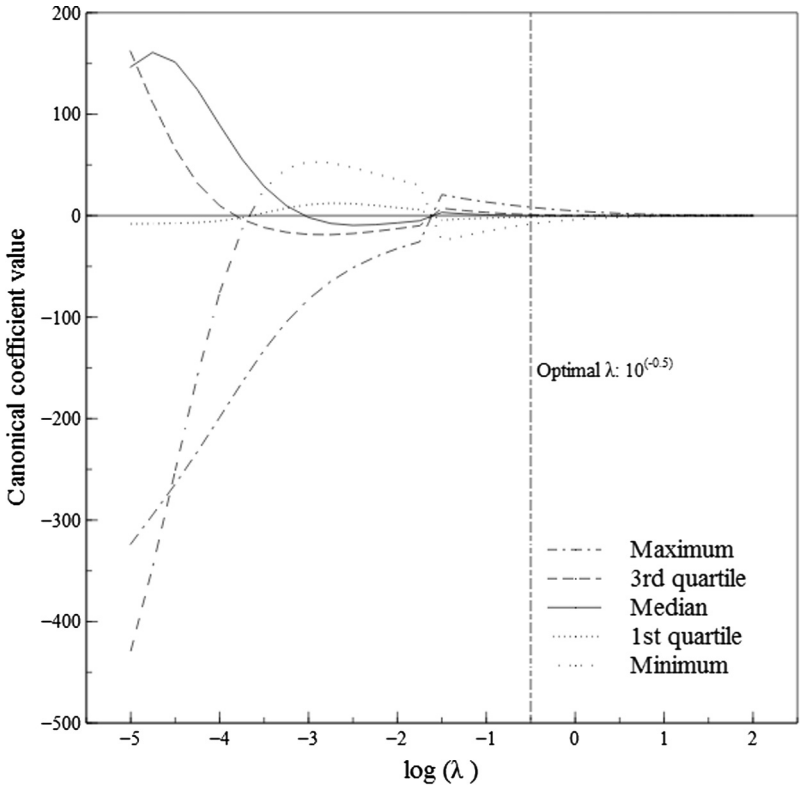

Fig. 3. Variation of coefficients of five selected features with changing λ in ridge PLDA (penalized linear discriminant analysis) applied on the enhanced feature set. The five features were selected to represent the range of coefficient values at the optimal λ value, i.e. the maximum, the third quantile, the median, the first quantile and the minimum.

Table 6
Confusion matrix of the crop types classified using the ridge PLDA (penalized linear discriminant analysis) with $\lambda = 10^{-0.5}$. Numbers are field counts (table margins: fractions) on the test set.

Class	Table Grape	Walnut	Peach	Avocado	Nectarine	Mandarin	User's accuracy	Overall accuracy
Table Grape	249	6	0	0	15	0	0.92	
Walnut	7	244	0	0	0	0	0.97	
Peach	20	0	972	0	0	0	0.98	
Avocado	0	0	0	46	0	0	1.00	
Nectarine	0	0	0	6	23	0	0.79	
Mandarin	0	0	0	0	0	110	1.00	
Producer's accuracy	0.90	0.98	1.00	0.89	0.61	1.00		
Overall accuracy								0.97

this crop, its producer's accuracy (61%) reveals that 39% of the pixels actually corresponding to nectarine were misclassified (omission error). Indeed, as seen from the nectarine column of the confusion matrix, two out of five fields actually corresponding to that crop were misclassified as table grape. On the other hand, on average, 21% of the fields classified as nectarine are in fact not nectarine (commission error) but avocado.

3.3. Interpretation of the coefficients

The calculation of coefficients of the enhanced feature set derived from the ridge PLDA with the lowest MER (Fig. 4) shows that the most influential predictors are mostly concentrated on the first two dates of the SITS. The largest coefficients are observed along the diagonal cells of the graph. This means that NDIs constructed with bands belonging to any of the image dates 1 and 2 separately were the most important to classify the crops of interest. The nine bands that carried the highest predictor weights were: band 4 from image dates 2 (10.19) and 1 (9.3), band 7 from image dates 2 (6.05) and 1 (5.79), band 5 from image date 2 (4.25), bands 5 and 6 from image date 1 (3.6 and 3.3, respectively), band 3 from image date 2 (2.54), and band 2 from image date 1 (2.47) (Table 7, Fig. 5). Averaging coefficients by band across the SITS, the highest predictor weights corresponded to bands 4 (2.71), bands 7 (2.03) and band 5 (1.12), and in each case the first two image dates contributed the most (Table 10, Fig. 6).

4. Discussion

4.1. LDA performance

Several machine learning techniques have performed well when applied on single multi-/hyperspectral images or greenness temporal profiles to classify crop types. Among these are decision trees (DTs) (Pal and Mather, 2003; Wardlow and Egbert, 2010; Zhong et al., 2011), support vector machine (SVM) (Melgani and Bruzzone, 2004; Pal and Mather, 2005) and random forest (RF) (Pal, 2005; Tatsumi et al., 2015; Zheng et al., 2015). Moreover, these techniques have yielded similar performances when compared in the classification of crop targets (Pal, 2005; Pal and

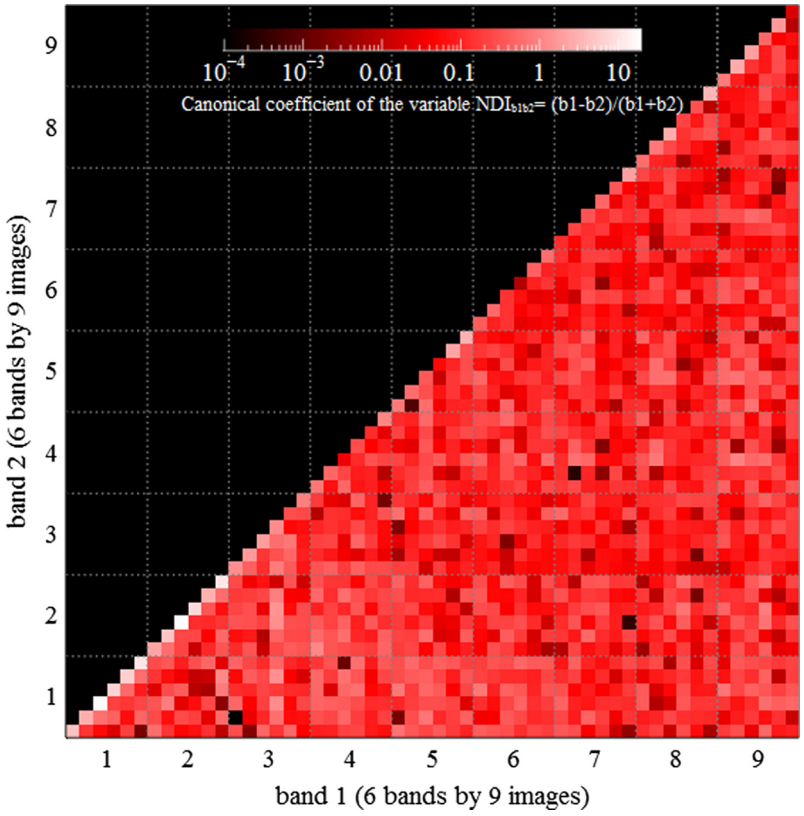

Fig. 4. Coefficients of the enhanced feature set derived from the ridge PLDA (penalized linear discriminant analysis) with optimal λ. Larger coefficients (brighter colors) correspond to more influential features; only absolute values are displayed. The *x* and *y* axes enumerate the nine images of the Landsat-8 time series; each one of them with six bands (from 2 to 7). The graph's cells display a coefficient for an NDI (normalized difference index) constructed from the bands identified by the *x* and *y* axes, or for a band itself (along the diagonal). (For interpretation of the references to colour in this figure legend, the reader is referred to the web version of this article.)

Table 7
Mean coefficients of the enhanced feature set derived from the ridge PLDA (penalized linear discriminant analysis) with optimal λ. The calculation considers the band itself and all related NDIs (normalized difference indices).

Image#	Mean by image band					
	2	3	4	5	6	7
1	2.47	1.56	9.3	3.63	3.3	5.79
2	1.25	2.54	10.19	4.25	1.6	6.05
3	0.75	0.94	1.05	0.77	0.24	0.54
4	0.49	0.34	0.16	0.23	0.13	0.62
5	0.5	0.37	0.32	0.11	1.21	1.69
6	0.29	0.33	0.17	0.08	0.27	0.38
7	0.13	0.18	0.25	0.31	0.22	1.08
8	0.38	0.46	1.45	0.18	0.19	1.78
9	0.52	1.43	1.12	0.37	0.94	0.08

Mather, 2005; Rodriguez-Galiano et al., 2012). In a setting that shares many similarities with this study, Peña and Brenning (2015) compared the performance of three state-of-the-art machine learning techniques (LDA, RF and SVM) on a Landsat-8 time series to classify four fruit-tree crops in a study area also placed in central Chile. Although good MERs were found for all the classifiers ($\leq$0.21), LDA had a slightly better performance, even using a training sample size as small as 200 fields (MER = 0.06). RF and SVM were furthermore computationally much more demanding, and SVM in particular was prohibitively slow for the larger sample sizes. Based on these findings, we decided to perform our classifications by only LDA, adding its lasso and ridge penalized variants to handle the high dimensionality of the enhanced feature set resulting from the spectrotemporal index construction.

LDA has shown a good trade-off between performance and computational complexity for a wide range of high-dimensional data sets (Li et al., 2006). It is relatively easy to implement as it does not require any parameter tuning unlike other machine learning techniques such as SVM. However, it is unsuitable for high-dimensional situations where the number of parameters is close to or greater than the number of observations, leading to an ill-posed problem. To deal with this shortcoming, regularized and penalized variants may be used, tuning the λ parameter to optimize the desired performance measure such as the MER.

For a set of ill-posed hyperspectral image classification experiments Bandos et al. (2009) found that regularized and penalized LDAs produced competitive results compared to a nonlinear SVM. Although in some cases the latter technique achieved somewhat higher overall classification accuracies, this basically occurred when the training set increased to more than 50 observations, turning less evident the ill-posed problem. Moreover, such accuracy improvements came at the cost of high computational cost

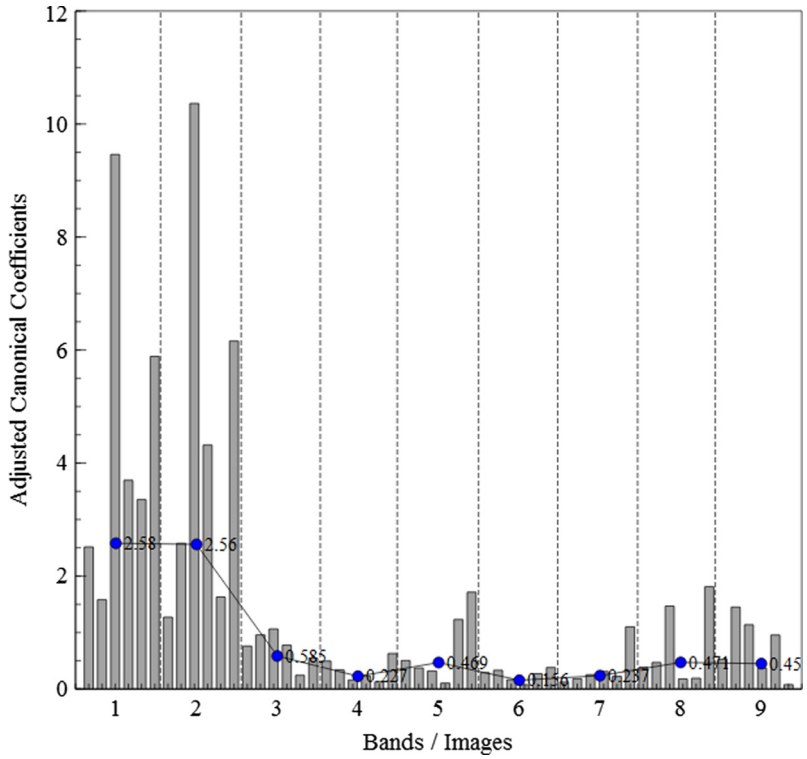

Fig. 5. Mean coefficients of each of the 54 bands comprising the Landsat-8 time series, derived from the ridge PLDA (penalized linear discriminant analysis) with optimal λ. The calculation considers the band itself and all related NDIs (normalized difference indices). Blue dots show mean coefficients averaged by image number. (For interpretation of the references to colour in this figure legend, the reader is referred to the web version of this article.)

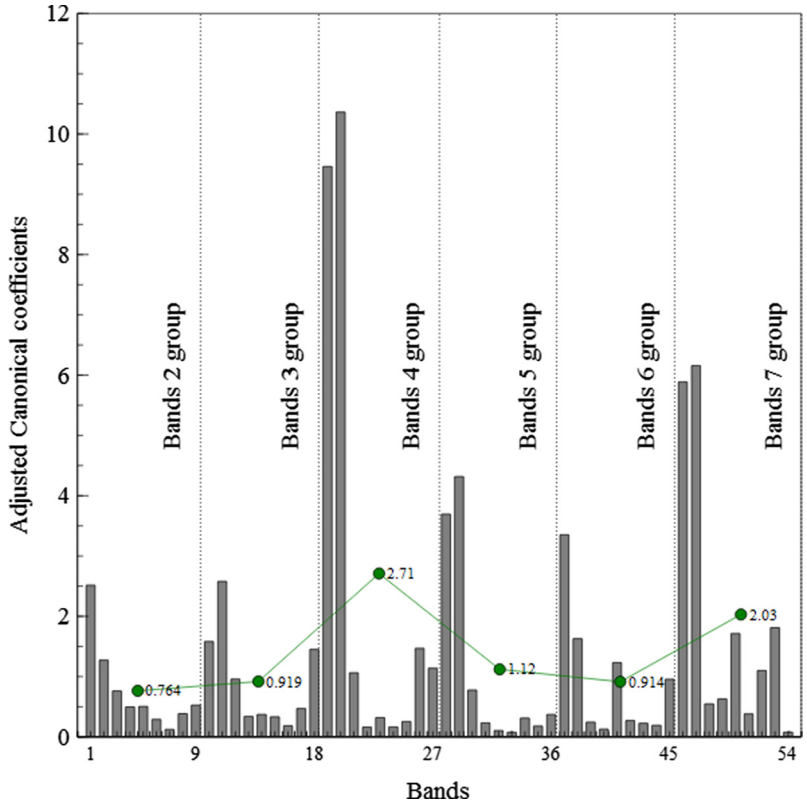

Fig. 6. Mean coefficients of each of the 54 bands comprising the Landsat-8 time series, derived from the ridge PLDA (penalized linear discriminant analysis) with optimal λ. The calculation considers the band itself and all related NDIs (normalized difference indices). Green dots show mean coefficients averaged by band. (For interpretation of the references to colour in this figure legend, the reader is referred to the web version of this article.)

associated with model selection, which gave an advantage to the LDA classifiers tested. Similarly, Yu et al. (1999) achieved classification accuracies of conifer species as high as those of neural networks (~90%) when two types of PLDA were applied on hyperspectral imagery. By analyzing the discriminant variables and λ parameter, they also identified the spectral regions carrying the largest predictor weights.

Peña and Brenning (2015) also found that using the full-band SITS, instead of just single image dates or NDVI/NDWI-based temporal profiles, reduced the overall MERs of the targeted fruit-tree crops by 4 and 13 percentage points, depending on the classifier and the training sample size used. We further explored the capabilities of SITS in this regard by using a novel approach in which a high-dimensional (enhanced) feature set comprising all the NDIs possible of being constructed from any two bands of the time series was tested to perform the classifications of interest. By doing this, overall MERs were reduced by between 3 and 20 percentage points depending on the LDA technique used (Table 5). The MER was one of the best (0.13) when the standard LDA was applied on the baseline feature set, but it was further improved by 3 percentage points and reached its lowest value (0.1) when the enhanced feature set, along with ridge PLDA, was used. In comparison, standard LDA produced somewhat worse results than the study of Peña and Brenning (2015), which may be related to the spectrally more demanding classification involved in our study, as six instead four crop types were targeted.

A possible reason for the better performance of ridge compared to lasso PLDA may be related to the type of coefficient shrinkage imposed. By using of the l_1 norm to measure the length of the coefficient vector, the lasso shrinks some of the coefficients to zero, effectively excluding the corresponding features from the model (James et al., 2013). The ridge, in contrast, shrinks coefficient values towards zero without forcing them to become exactly zero. Thus, all features will still be used as part of a weighted sum, and we argue that this averaging of variables that are individually affected by noise may reduce the effect of band-specific noise and thus help extract useful information from large feature sets. Lasso, in contrast, would be more promising in situations where only a small subset of features contributes to predicting the response, while the remaining features are largely irrelevant (Hastie et al., 2009). In many remote sensing applications, however, a large number of features is expected to show at least some correlation to the property of interest (e.g., Peña et al., 2012).

Several other shrinkage methods have been proposed especially for linear regression and may warrant further investigation also in an LDA context. Nevertheless, regularization based on partial least squares (PLS) and principal components analysis (PCA) tend to be similar to but less stable than ridge penalties (Hastie et al., 2009). While ridge and lasso penalize smoothly as a function of λ, PLS and PCA penalize in discrete steps (e.g., by adding one principal component after another), which leads to a coarser model selection (Hastie et al., 2009).

4.2. Feature importance

As it follows from the introduction chapter, most of the SITS-based crop type classifications have commonly used NDVI temporal profiles as feature set, thus relating the class membership to a unique and temporally fixed arithmetic band combination based on red and NIR bands corresponding to the same image date. Although this approach has yielded good results, Peña and Brenning (2015) demonstrated that better classification accuracies may be achieved using the full-band SITS, and as demonstrated here, they may be further improved if a spectrotemporal NDI-based feature set is constructed from that time series. Moreover, our findings show that red and NIR bands, commonly used to construct greenness spectral indices like the NDVI, were not the only important predictors across the SITS. While the red band had the highest predictor weight, it was followed by the SWIR band at 2.11–2.19 μm, with the NIR band ranked in the third position (Table 7, Fig. 5). All these bands had especially high weights along the first two image dates of the time series (Table 7, Fig. 5). Similar findings were reported by Peña and Brenning (2015), who found the red and SWIR bands (centered at 1.57–1.65 μm) of the first image date of the time series used as the most relevant for fruit-tree crop type classification. Previous classifications performed on diverse annual and perennial crops by NDVI temporal profiles reported that the best spectrotemporal separabilities between crop types occur at their earlier and later phenological stages, as a result of their specific planting and harvesting dates (Zheng et al., 2015). Despite specific information about the planting calendars of the crops of interest was not able for the current study, differences in the vegetation cover of its fields were apparent at the earlier image dates of the time series, which should maximize their discrimination.

The predictive importance of the red bands found in our study suggests that differences in the photosynthetic activity of the crops of interest were especially apparent at the beginning of the growing season, which should be explained by the dissimilar onset of their greenup stages. Similarly, the predictive importance of the SWIR band at 2.11–2.19 μm band indicates that differences in the crop's foliar turgor were also more apparent at the beginning of the growing season, but interestingly they were not detected by the SWIR band at 1.57–1.65 μm. Typically, this band of the Landsat sensors produces stronger and less noisy water absorption features, which is why it has been preferred to construct water spectral indices such as the NDWI (Gao, 1996). As a matter of fact, many NDWIs derived from spaceborne optical sensors are similarly constructed, using a SWIR band placed at the beginning of this spectral region (1.24–1.65 μm) rather than at the end (Ceccato et al., 2002; Zarco-Tejada et al., 2003; Yilmaz et al., 2008). Nonetheless, in our study case such absorption features appear to be relatively less developed or behaved relatively unstably during the earlier phenological stages of the crops of interest. Although ranked somewhat below the red and SWIR bands, the NIR band had also a high predictive value, suggesting that differences in the crops' foliage amount were also especially apparent at the beginning of the growing season, thus favoring the crop classification.

5. Conclusions

We classified six fruit-tree crop types by applying LDA techniques on a Landsat-8 time series corresponding to the 2014–15 growing season. Although LDA applied on the full-band SITS yielded good classification accuracies (MER = 0.13), they were further improved by 23% (MER = 0.10) when all NDIs possible of being constructed from the SITS were used. Accordingly, spectrotemporal indices as constructed here may contribute to increasing the accuracy of SITS-based crop type classifications. Until now, these indices have been mainly constructed by arithmetically combining two bands of the same image date in order to derive greenness spectral indices profiles like those from the NDVI. Furthermore, this spectrotemporal NDI-based feature set could be also tested to classify any type of targets whose temporal variability justifies the use of SITS.

The most important bands to classify the crops of interest were concentrated on the first two image dates of the time series, where differences in the crops' greenup stage maximize their chances of being spectrally discriminated. These finding points towards the image dates that should be prioritized to construct spectrotemporal

indices intended to classify this type of targets. Despite the high feature weights provided by the red and NIR bands, used to construct the typical greenness spectral indices like the NDVI, several other bands were also found important for the pursued classification. By measuring the importance of each image band in the classification procedure we assessed the usefulness of the complete spectral resolution of the time series in the construction of spectrotemporal indices.

Further improvements in the methodology exposed here could be carried out by constructing time series with higher spatial resolution images, thus including the classification of smaller crop fields. As technical properties of the satellite-based optical sensors are progressing the availability of images with fine pixel sizes holding a similar spectral resolution and bandwidth to the Landsat series' sensors will be possible, like those acquired by the recently launched Sentinel-2 Earth-observing satellites.

Acknowledgements

This research was partly funded through an NSERC (Natural Sciences and Engineering Research Council of Canada) Discovery Grant awarded to A. Brenning.

References

Arvor, D., Jonathan, M., Simões, M., Meirelles, P., Dubreuil, V., Durieux, L., 2011. Classification of MODIS EVI time series for crop mapping in the state of Mato Grosso, Brazil. Int. J. Remote Sens. 32 (22), 7821–7847.

Badhwar, G.D., Gargantini, C.E., Redondo, F.V., 1987. LANDSAT classification of Argentina summer crops. Remote Sens. Environ. 21, 111–117.

Bandos, T.V., Bruzzone, L., Camps-Valls, G., 2009. Classification of hyperspectral images with regularized linear discriminant analysis. IEEE Trans. Geosci. Remote Sens. 47 (3), 862–873.

Bioucas-Dias, J.M., Plaza, A., Camps-Valls, G., Scheunders, P., Nasrabadi, N.M., Chanussot, J., 2013. Hyperspectral remote sensing data analysis and future challenges. IEEE Geosci. Remote Sens. 1 (2), 6–36.

Brenning, A., 2009. Benchmarking classifiers to optimally integrate terrain analysis and multispectral remote sensing in automatic rock glacier detection. Remote Sens. Environ. 113 (1), 239–247.

Brenning, A., 2012. Spatial cross-validation and bootstrap for the assessment of prediction rules in remote sensing: The R package 'sperrorest'. In: 2012 IEEE International Geoscience and Remote Sensing Symposium (IGARSS), 23–27 July 2012, pp. 5372–5375.

Ceccato, P., Flasse, S., Gregoire, J., 2002. Designing a spectral index to estimate vegetation water content from remote sensing data: Part 2. Validation and applications. Remote Sens. Environ. 82, 198–207.

Ceccato, P., Flasse, S., Tarantola, S., Jacquemoud, S., Grégoire, J.-M., 2001. Detecting vegetation leaf water content using reflectance in the optical domain. Remote Sens. Environ. 77, 22–33.

Chen, Z., Li, S., Ren, J., Gong, P., Zhang, M., Wang, L., Xiao, S., Jiang, D., 2008. Monitoring and management of agriculture with remote sensing. In: Liang, S. (Ed.), Advances in Land Remote Sensing—System, Modelling, Inversion and Adaptation. Springer, University of Maryland, USA, pp. 397–421.

Chenab, C.F., Sonb, N.T., Changab, L.Y., Chenb, C.R., 2011. Classification of rice cropping systems by empirical mode decomposition and linear mixture model for time-series MODIS 250 m NDVI data in the Mekong Delta, Vietnam. Int. J. Remote Sens. 32 (18), 5115–5134.

CIREN (Centro de Información de Recursos Naturales), 2014. Actualización catastro frutícula Región de Valparaíso. Santiago: CIREN, 105 pp.

Esch, T., Metz, A., Marconcini, M., Keil, M., 2014. Combined use of multi-seasonal high and medium resolution satellite imagery for parcel-related mapping cropland and grassland. Int. J. Appl. Earth Obs. Geoinf. 28, 230–237.

Du, Q., Younan, N.H., 2008. Dimensionality reduction and linear discriminant analysis for hyperspectral image classification. In: Lovrek, I., Howlett, R.J., Jain, L. C. (Eds.), Knowledge-Based and Intelligent Information and Engineering Systems. Springer, Berlin, pp. 392–399.

Gao, B., 1996. NDWI—A normalized difference water index for remote sensing of vegetation liquid water from space. Remote Sens. Environ. 58 (3), 257–266.

Gómez, C., White, J.C., Wulder, M.A., 2016. Optical remotely sensed time series data for land cover classification: a review. ISPRS J. Photogramm. Remote Sens. 116, 55–72.

Hastie, T., Tibshirani, R., Buja, A., 1994. Flexible discriminant-analysis by optimal scoring. J. Am. Statist. Assoc. 89 (428), 1255–1270.

Hastie, T., Buja, A., Tibshirani, R., 1995. Penalized discriminant analysis. Ann. Stat. 23 (1), 73–102.

Hastie, T., Tibshirani, R., Friedman, J., 2009. The Elements of Statistical Learning: Data Mining, Inference, and Prediction. Springer, New York. 763 pp.

INE (Instituto Nacional de Estadísticas), 2008. Proyecto Aconcagua, Informe final 2008. Santiago: Gobierno de Chile SERCOTEC, 81 pp.

Jakubauskas, M.E., Legates, D.R., Kastens, H., 2002. Crop identification using harmonic analysis of time-series AVHRR NDVI data. Comput. Electron. Agric. 37, 127–139.

James, G., Witten, D., Hastie, T., Tibshirani, R., 2013. An Introduction to Statistical Learning With Applications in R. Springer, New York. 426 pp.

Jewell, N., 1989. An evaluation of multi-date SPOT data for agriculture and land use mapping in the United Kingdom. Int. J. Remote Sens. 10, 939–951.

Jones, H., Vaughan, R., 2010. Remote Sensing of Vegetation: Principles, Techniques and Applications. Oxford University Press, New York. 353 pp.

Li, T., Zhu, S., Ogihara, M., 2006. Using discriminant analysis for multi-class classification: an experimental investigation. Knowl. Inf. Syst. 10 (4), 453–472.

Lo, T.H.C., Scarpace, F.L., Lillesand, T.M., 1986. Use of multitemporal spectral profiles in agricultural land-cover classification. Photogramm. Eng. Remote Sens. 52 (4), 535–544.

Mahlein, A.-K., Rumpf, T., Welke, P., Dehne, H.-W., Plümer, L., Steiner, U., Oerke, E.-C., 2013. Development of spectral indices for detecting and identifying plant diseases. Remote Sens. Environ. 128, 21–30.

Masialeti, I., Egbert, S., Wardlow, B.D., 2010. A comparative analysis of phenological curves for major crops in Kansas. GI Sci. Remote Sens. 47 (2), 241–259.

McCoy, R.M., 2005. Field Methods in Remote Sensing. The Guilford Press, New York. 159 pp.

Melgani, F., Bruzzone, L., 2004. Classification of hyperspectral remote sensing images with support vector machines. IEEE Trans. Geosci. Remote Sens. 42 (8), 1778–1790.

Mingwei, Z., Qingbo, Z., Zhongxin, C., Jia, L., Yong, Z., Chongfa, C., 2008. Crop discrimination in northern China with double cropping systems using Fourier analysis of time-series MODIS data. Int. J. Appl. Earth Obs. Geoinf. 10, 476–485.

Mountrakis, G., Im, J., Ogole, C., 2011. Support vector machines in remote sensing: A review. ISPRS J. Photogramm. Remote Sens. 66, 247–259.

Murakami, T., Ogawa, S., Ishitsuka, K., Kumagai, K., Saito, G., 2001. Crop discrimination with multitemporal SPOT/HRV data in the Saga Plains, Japan. Int. J. Remote Sens. 22 (7), 1335–1348.

Odenweller, J.B., Johnson, K.I., 1984. Crop identification using Landsat temporalspectral profiles. Remote Sens. Environ. 14 (1–3), 39–54.

Ozdogan, M., 2010. The spatial distribution of crop types from MODIS data: Temporal unmixing using independent component analysis. Remote Sens. Environ. 114, 1190–1204.

Pal, M., 2005. Random forest for classification in remote sensing. Int. J. Remote Sens. 26 (1), 217–222.

Pal, M., Mather, P.M., 2003. An assessment of the effectiveness of decision tree methods for land cover classification. Remote Sens. Environ. 86, 554–565.

Pal, M., Mather, P.M., 2005. Support vector machines for classification in remote sensing. Int. J. Remote Sens. 26 (5), 1007–1011.

Peña, M.A., Brenning, A., 2015. Assessing fruit-tree crop classification from Landsat-8 time series for the Maipo Valley, Chile. Remote Sens. Environ. 171, 234–244.

Peña, M.A., Brenning, A., Sagredo, A., 2012. Constructing satellite-derived hyperspectral indices sensitive to canopy structure variables of a Cordilleran Cypress (*Austrocedrus chilensis*) forest. ISPRS J. Photogramm. Remote Sens. 74, 1–10.

R Core Team, 2014. R: A language and environment for statistical computing. Vienna, Austria: R Foundation for Statistical Computing (URL http://www.R-project.org/).

Rodriguez-Galiano, V.F., Ghimire, B., Rogan, J., Chica-Olmo, M., Rigol-Sanchez, J.P., 2012. An assessment of the effectiveness of a random forest classifier for land-cover classification. ISPRS J. Photogramm. Remote Sens. 67, 93–104.

Roy, D.P., Wulder, M.A., Loveland, T.R., Woodcock, C.E., Allen, R.G., Anderson, M.C., Helder, D., Irons, J.R., Johnson, D.M., Kennedy, R., Scambos, T.A., Schaaf, C.B., Schott, J.R., Sheng, Y., Vermote, E.F., Belward, A.S., Bindschadler, R., Cohen, W.B., Gao, F., Hipple, J.D., Hostert, P., Huntington, J., Justice, C.O., Kilic, A., Kovalskyy, V., Lee, Z.P., Lymburner, L., Masek, J.G., McCorkel, J., Shuai, Y., Trezza, R., Vogelmann, J., Wynne, R.H., Zhu, Z., 2014. Landsat-8: science and product vision for terrestrial global change research. Remote Sens. Environ. 145, 154–172.

Sakamoto, T., Yokozawa, M., Toritani, H., Shibayama, M., Ishitsuka, N., Ohno, H., 2005. A crop phenology detection using time-series MODIS data. Remote Sens. Environ. 96, 366–374.

Shao, J., Lunetta, R.S., Ediriwickrema, J., Liames, J., 2010. Mapping cropland and major crop types across the Great Lakes Basin using MODIS-NDVI data. Photogramm. Eng. Remote Sens. 75 (1), 73–84.

Sibanda, M., Murwira, A., 2012. The use of multi-temporal MODIS images with ground data to distinguish cotton from maize and sorghum fields in smallholder agricultural landscapes of southern Africa. Int. J. Remote Sens. 33 (16), 4841–4855.

Simonneaux, V., Duchemin, B., Helson, D., Er-Raki, S., Olioso, A., Chehboun, A.G., 2007. The use of high-resolution image time series for crop classification and evapotranspiration estimate over an irrigated area in central Morocco. Int. J. Remote Sens. 29 (1), 95–116.

Sun, H., Xu, A., Lin, H., Zhang, L., Mei, Y., 2012. Winter wheat mapping using temporal signatures of MODIS vegetation index data. Int. J. Remote Sens. 33 (16), 5026–5042.

Tatsumi, K., Yamashiki, Y., Canales Torres, M.A., Taipe, C.L.R., 2015. Crop classification of upland fields using Random forest of time-series Landsat 7 ETM+ data. Comput. Electron. Agric. 115, 171–179.

Turker, M., Arikan, M., 2005. Sequential masking classification of multi-temporal Landsat7 ETM+ images for field-based crop mapping in Karacabey, Turkey. Int. J. Remote Sens. 26 (17), 3813–3830.

Van Niel, T.G., McVicar, T.R., 2004. Determining temporal windows for crop discrimination with remote sensing: a case study in south-eastern Australia. Comput. Electron. Agric. 45 (1–3), 91–108.

Wardlow, B., Egbert, S., 2010. A comparison of MODIS 250-m EVI and NDVI data for crop mapping: a case study for southwest Kansas. Int. J. Remote Sens. 31 (3), 805–830.

Witten, D., 2015. Penalized Classification using Fisher's Linear Discriminant (URL http://cran.r-project.org/package=penalizedLDA).

Witten, D.M., Tibshirani, R., 2011. Penalized classification using Fisher's linear discriminant. *Journal of the Royal Statistical Society. Series B*. Statist. Methodol. 73 (5), 753–772.

Xavier, A.C., Rudorff, B.F.T., Shimabukuro, Y.E., Berka, L.M.S., Moreira, M.A., 2006. Multi-temporal analysis of MODIS data to classify sugarcane crop. Int. J. Remote Sens. 27 (4), 755–768.

Yilmaz, M.T., Hunt Jr., E.R., Jackson, T.J., 2008. Remote sensing of vegetation water content from equivalent water thickness using satellite imagery. Remote Sens. Environ. 112, 2514–2522.

Yu, B., Ostland, M., Gong, P., Pu, R., 1999. Penalized discriminant analysis of *in situ* hyperspectral data for conifer species recognition. IEEE Trans. Geosci. Remote Sens. 37 (5), 2569–2577.

Zarco-Tejada, P.J., Rueda, C.A., Ustin, S.L., 2003. Water content estimation in vegetation with MODIS reflectance data and model inversion methods. Remote Sens. Environ. 85, 109–124.

Zheng, B., Myint, S.W., Thenkabail, P.S., Aggarwal, R.M., 2015. A support vector machine to identify irrigated crop types using time-series Landsat NDVI data. Int. J. Appl. Earth Obs. Geoinf. 34, 103–112.

Zhong, L., Gong, P., Biging, G., 2014. Efficient corn and soybean mapping with temporal extendability: a multi-year experiment using Landsat imagery. Remote Sens. Environ. 140, 1–13.

Zhong, L., Hawkins, T., Biging, G., Gong, P., 2011. A phenology-based approach to map crop types in the San Joaquin Valley, California. Int. J. Remote Sens. 32 (22), 7777–7804.